

Landslides (2022) 19:1913–1934
 DOI 10.1007/s10346-022-01903-w
 Received: 3 November 2021
 Accepted: 12 May 2022
 Published online: 25 May 2022
 © Springer-Verlag GmbH Germany,
 part of Springer Nature 2022

Fawu Wang · Kongming Yan  · Kounghoon Nam · Guolong Zhu ·
 Xingliang Peng · Zixin Zhao



The Wuxie debris flows triggered by a record-breaking rainstorm on 10 June 2021 in Zhuji City, Zhejiang Province, China

Abstract Deep into the night of 9 June 2021, a high-intensity and short-duration rainstorm, the largest rainfall ever recorded in Zhuji, struck the entire city. The abrupt rainfall triggered several debris flows, which killed four residents and closed a highly ranked national scenic area for over three months. The debris flows, triggered by record-breaking rainfall, occurred in a rhyolite porphyry area that was not recognised as an area prone to frequent debris flow. Thus, detailed field investigations were conducted on three debris flow gullies. It was demonstrated that an extreme rainfall event, complex topographic profiles and abundant diluvium in the gullies were the main contributing factors in the disastrous damage. In particular, steep eluvial slopes with a high gradient of over 30° failed under heavy rainfall, which was one of the major factors in the initiation of debris flows. In addition, geometric properties, such as the curved travelling path, natural cliff and cross-sectional shape of the gullies, interacted significantly with the deep and lateral erosions of diluvium in the gullies, which promoted mass enlargement and the long-runout movement of the debris flows. Furthermore, reasonable countermeasures made some contribution to the reduction and mitigation of this kind of geo-disasters.

Keywords Geo-disaster · Debris flow · Heavy rainfall · Rhyolite porphyry · Field investigation

Introduction

A debris flow is a common and unique geo-hazard in mountainous regions, which usually causes incalculable economic losses and catastrophic numbers of casualties (Jeong et al. 2015; Yang et al. 2015a, b; Chang et al. 2020). The triggering mechanisms and motion characteristics of debris flow in various geological configurations have been studied widely by researchers all over the world (Samodra et al. 2018; Setiawan et al. 2019). There is no doubt that heavy rainfall is the main triggering factor for initial slope failures, as illustrated in several studies using different methods (Wang et al. 2015; Doglioni et al. 2020; Zhao et al. 2021). Lithological properties are another key factor in the initiation of debris flow (Achu et al. 2021). In addition to triggering characteristics, debris flow involves several complex processes, such as transformation, particle segregation and deposition with complex topographic features (Igwe et al. 2006; Peng et al. 2015; Zhou et al. 2015; Hotta et al. 2021; Guo et al. 2020). These factors are usually simplified or ignored in experimental modelling and numerical simulations (McFall et al. 2018; Cuomo 2020). In this situation, a failed case with various geological

characteristics is explored to improve the understanding of this type of geo-disaster.

On the night of 9 June 2021, an abrupt rainstorm with high intensity and short duration hit the city of Zhuji in Zhejiang Province, China. This local record-breaking rainfall event triggered over 100 mass movements, including debris flows and landslides. Most were in a specified area surrounding a famous Chinese national tourist attraction, the Wuxie scenic area. The debris flow caused four deaths, destroyed four houses, damaged at least 10 buildings and severely damaged the national tourist attraction, causing it to close for over three months. In this case, one of the interesting phenomena is that these debris flows were derived in a rhyolite porphyry formation, as well as impact of the record-breaking heavy rainfall. Generally, easily weathered lithological formations, such as granite, are prone to fluidised mass movements (Wang et al. 2003, 2015). However, the susceptibility to debris flow in a rhyolite porphyry formation, a kind of extrusive igneous rock formation with strong anti-weathering capability, is an important topic for the prevention of future geo-disasters.

Over a period of 2 months after the incident, to understand the initiation and motion mechanisms of these debris flows, detailed surveys equipped with an unmanned air vehicle (UAV) were carried out three times on three major debris flow gullies. During these investigations, we collected geological information and rainfall data, analysed the possible triggering mechanisms and movement characteristics of debris flows and discussed potential countermeasures for the prevention and reduction of disasters caused by the debris flows. This report provides practical data about debris flows and seeks to improve local residents' and governmental understanding of geo-disaster reduction.

Overview of debris flows

Area setting

The group-occurring debris flows, designated as 'the Wuxie debris flows' in this paper, occurred in the Wuxie scenic area in Zhuji, Zhejiang, Southeast China. Zhejiang, one of the most economically developed and highly dense populated provinces in China, is frequently struck by mass movements, which can cause enormous economic losses. The Wuxie scenic area is a national four-star (second-highest rank) tourist attraction in China. It is situated less than 20 km from Zhuji and about 60 km from Hangzhou, the capital city of Zhejiang Province (see Fig. 1). In the Wuxie scenic area, there is a

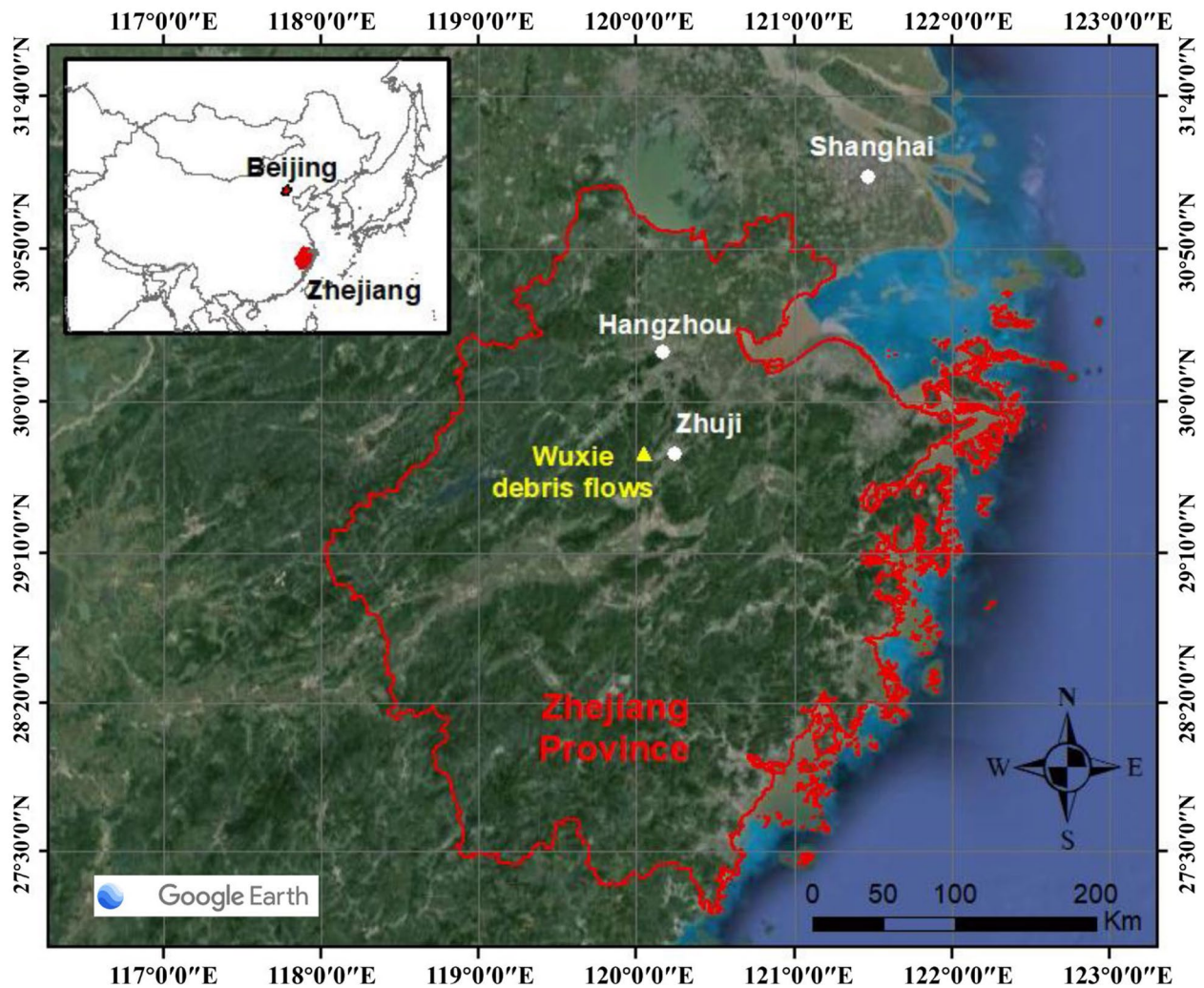


Fig. 1 The location of the Wuxie debris flows in Zhejiang Province, Southeast China. The position of the Wuxie debris flows is represented by that of the tourist service centre, which is close to the debris flow gullies and the meteorological station (WXSK) marked in Fig. 2

reservoir called the Wuxie reservoir. It has a storage capacity of 10 million m^3 , making it important for the entire city of Zhuji.

Debris flow distribution in the study area

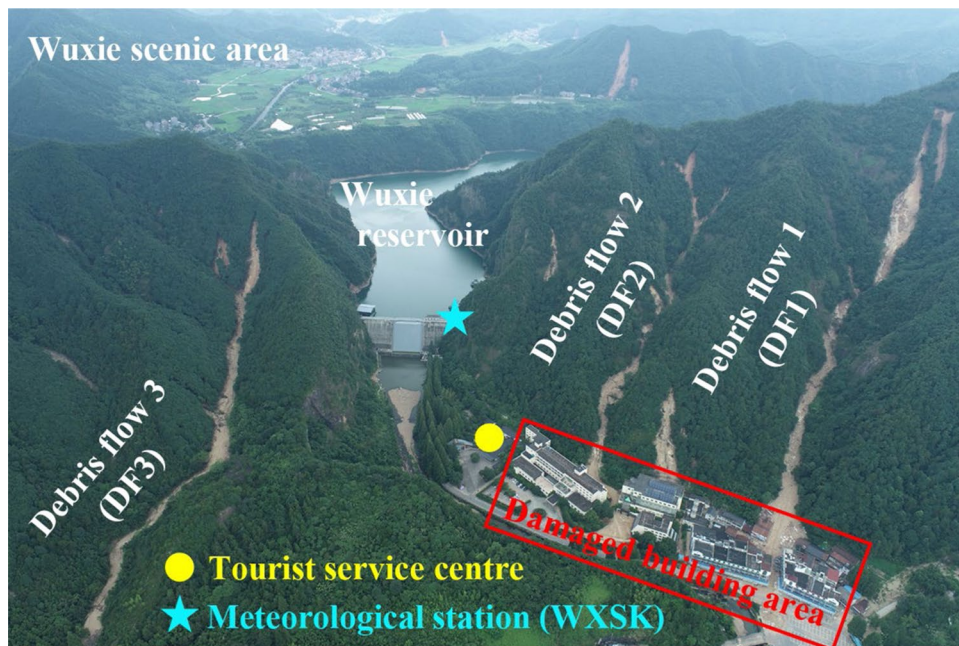
The Wuxie scenic area was observed to have had enormous rain-storm-triggered debris flows surrounding the Wuxie reservoir, as shown in Fig. 2. Among them, three typical debris flows shown in Fig. 2 were selected as the main targets for our investigation and designated as DF1, DF2 and DF3, respectively. Two of them, DF1 and DF2, occurred on the left side of the Wuxie reservoir, while the third, DF3, occurred on the right side. They were detected by aerial photography, as shown in Fig. 3. From these figures, a large residential building area in front of the tourist service centre was severely damaged by DF1 and DF2. A detailed account of the disastrous

damage caused alongside major fatalities and major economic losses in this area will be introduced in the following section.

Disastrous damage in the deposition area

In the study area, DF1 and DF2 caused damage and major casualties. Among the two, DF1 was the largest and longest. The four deaths, four destroyed houses and the most damaged and buried buildings were caused by DF1 (see Fig. 4). Figure 4a shows the four destroyed buildings, which are similar to the house shown in Fig. 4e, were entirely displaced. Meanwhile, several residential buildings were damaged or even crushed at positions (b)–(f) in Fig. 4a. Additionally, two local three-storey restaurants with narrow spacings between them were buried to a depth of about 3 m, as illustrated in Fig. 4g to j.

Fig. 2 Overview of the Wuxie debris flows



DF2 severely damaged the local Bairui Hotel, which included a five-storey main building and a three-storey attached building, as shown in Fig. 5. In this case, most of the debris, with an estimated height of about 3 m, was deposited behind the main building (see Fig. 5b to c), except for a few fine grain depositions in front of the buildings (see Fig. 5d). In addition to the direct damage, the Wuxie scenic area, a highly ranked national tourist attraction in Zhejiang Province, was closed for over three months, indirectly causing countless economic losses for local tourism development.

Precipitation, geological settings and soil properties

Precipitation

Zhejiang is a coastal province that is heavily affected by typhoons and plum rain. Compared with the short duration of the typhoon period, the plum rain season typically lasts 2 months on average. The plum rain season is specific to East Asia and is marked by frequent rainstorms (Zheng et al. 2020). According to the historical

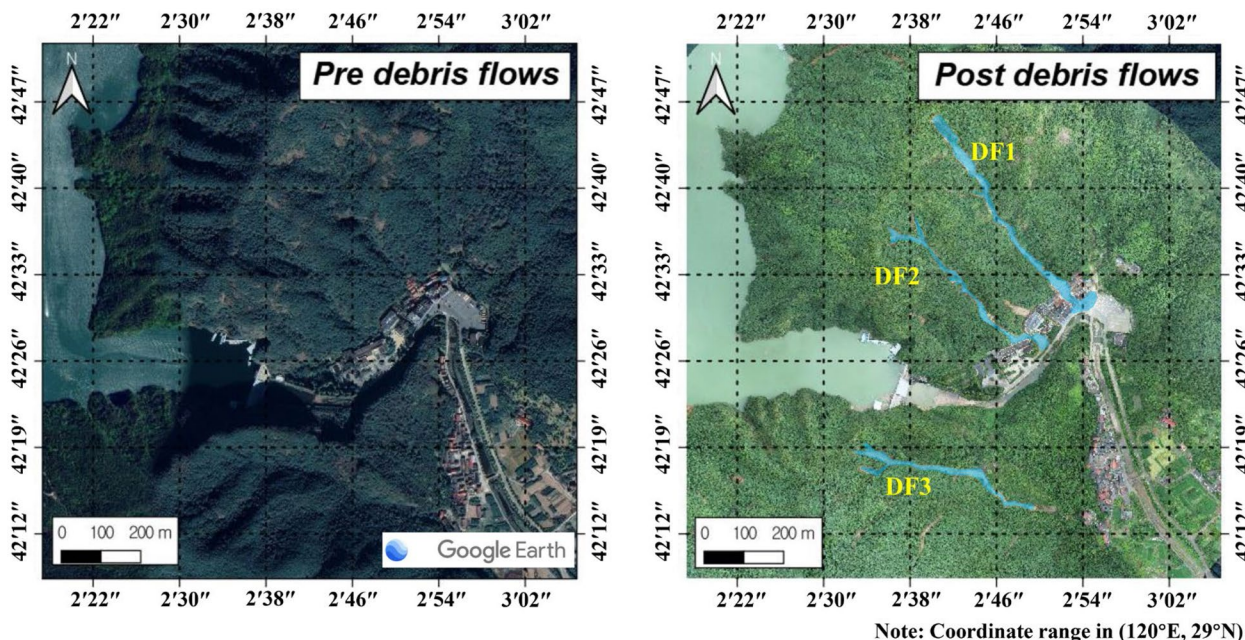
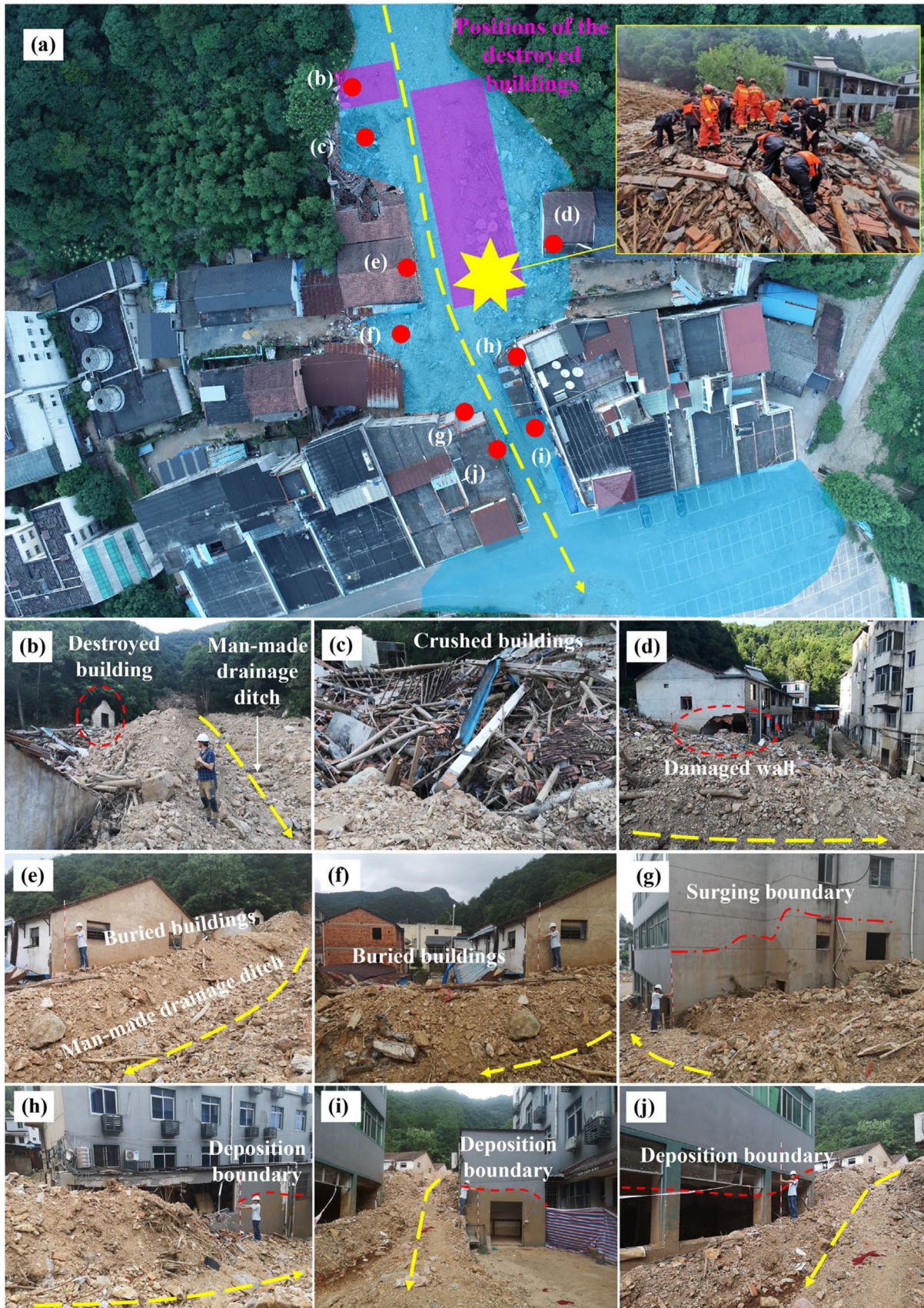


Fig. 3 Comparison of pre-(left) and post-(right) debris flows in the study area. The image of the pre-debris flows image was cropped from Google Earth, while the post-debris flow image was reconstructed by UAV modelling, with blue areas indicating the debris flows



◀**Fig. 4** Deposition area and damage caused by DF1, including top view of deposition area (a) and detailed features of the damaged buildings (b–j). The broken yellow line with an arrow represents the downstream direction of the debris flow, hereinafter the same. The photo outlined in yellow overlying (a) shows the rescue activity, which was collected from <https://xw.qq.com/cmsid/20210610A0AYGP00>

record, the average start date of the plum rain season in Zhejiang Province is 10 June. The debris flows that occurred this year corresponded precisely with the average start date.

The precipitation data provided by the Zhuji Water Resource Bureau illustrate the hourly and cumulative rainfall in Fig. 6. In this figure, the meteorological station WSK is the nearest station to the debris flow gullies investigated in this study (see Fig. 2). According to rainfall data, this high-intensity rainstorm occurred primarily over 4 h from 20:00 (9 June) to 00:00 (10 June) at this local area, and its 4-h cumulative rainfall reached 178 mm. In particular, the maximum hourly rainfall reached 109 mm at 00:00 (local time) on 10 June, the time at which most of the debris flows occurred.

In addition to the specific regional rainfall situation, according to local public news (<https://xw.qq.com/cmsid/20210610A0AYGP00>), the entire city of Zhuji suffered an abrupt and heavy rainstorm from 21:00 on 9 June to 1:00 on 10 June. The average hourly rainfall across the whole city was 60.5 mm, and the 6-h cumulative rainfalls in most meteorological stations were over 200 mm, the highest values ever recorded in Zhuji. According to the local meteorological management department, this record-breaking rainfall might occur only once every 100 years. It is reasonably estimated that these debris flows were triggered mainly by abrupt and extremely heavy rainstorms.

Geological settings

Geological settings, including tectogenesis, topography and lithology, are the primary factors that control the initiation mechanism and recurrence period of debris flows. In this case, geological maps, contour maps and joint statistics were collected from the geological database and the field investigations, which are shown in Figs. 7 and 8.

Regional geological configurations

The study area shown in Fig. 7 (outlined in yellow) was surrounded by several faults. Additionally, lithologic formations close to the area in its southeast (SE) direction were much more complex, indicating that this region had active tectonic activities in its geological history. Furthermore, the geological map indicates that there were two main lithologic formations inside the study area, $\gamma\omega J_3Z^b$ and J_3Z^a . The main lithologies of these two formations were rhyolitic tuff and rhyolite porphyry, respectively. It is unusual that so many debris flows occurred at the rhyolite porphyry formation because of their high anti-weathering capability. Rhyolite porphyry is an extrusive, igneous rock that erupts from volcanoes. Because it solidifies on the surface of the Earth, it is adaptive to the atmospheric environment and is more stable than intrusive igneous rock, such as granite (Plummer et al. 2015). This might be the main reason why the study area was not recognised in the past as a region

prone to fluidised mass movements, which was supported by the elderly residents as well. According to interviews with these long-time residents, they had never witnessed or heard about debris flow occurring at this site before.

To understand the degree of rock fragmentation, an important geological property of the debris flow gullies, a joint statistic on a side bank of the DF1 gully (at J1 in Fig. 9) was carried out and is shown in Fig. 8 as a representative example. In this case, there were six joints with an estimated spacing of about 50 to 200 mm in three main dip directions, as illustrated by the rose diagram in Fig. 8b.

Topography

Most of the areas in Zhejiang Province are surrounded by mountains, which is a significant topographic factor contributing to slope failure and mass movement. In the study area, the topographic map is represented by a contour map in Fig. 9, which was calculated using the structure from motion (SfM) method with UAV image data. The results indicated that the highest elevations of the DF1 and DF2 source areas were about 380 m and 320 m, respectively, while their deposition front was about 120 m above sea level. The elevation differences of the DF1 and DF2 gullies were about 260 m and 200 m, respectively. However, the height of DF3 is only 120 m, from 260 m at the top of the gully to 140 m at the deposition front. In this case, the slope of DF3 is obviously smaller than that of DF1 and DF2; however, DF3 still has a long-runout distance. It has been demonstrated that the topography of the gully can have varied effects on specific types of debris flow. In addition, the water catchment boundary, an important factor in the long-runout movement of debris flows, was sketched onto the contour map (Fig. 9). In this case, all investigated gullies, especially the DF3 gully, had a large water catchment with a gentle gully slope.

Soil properties

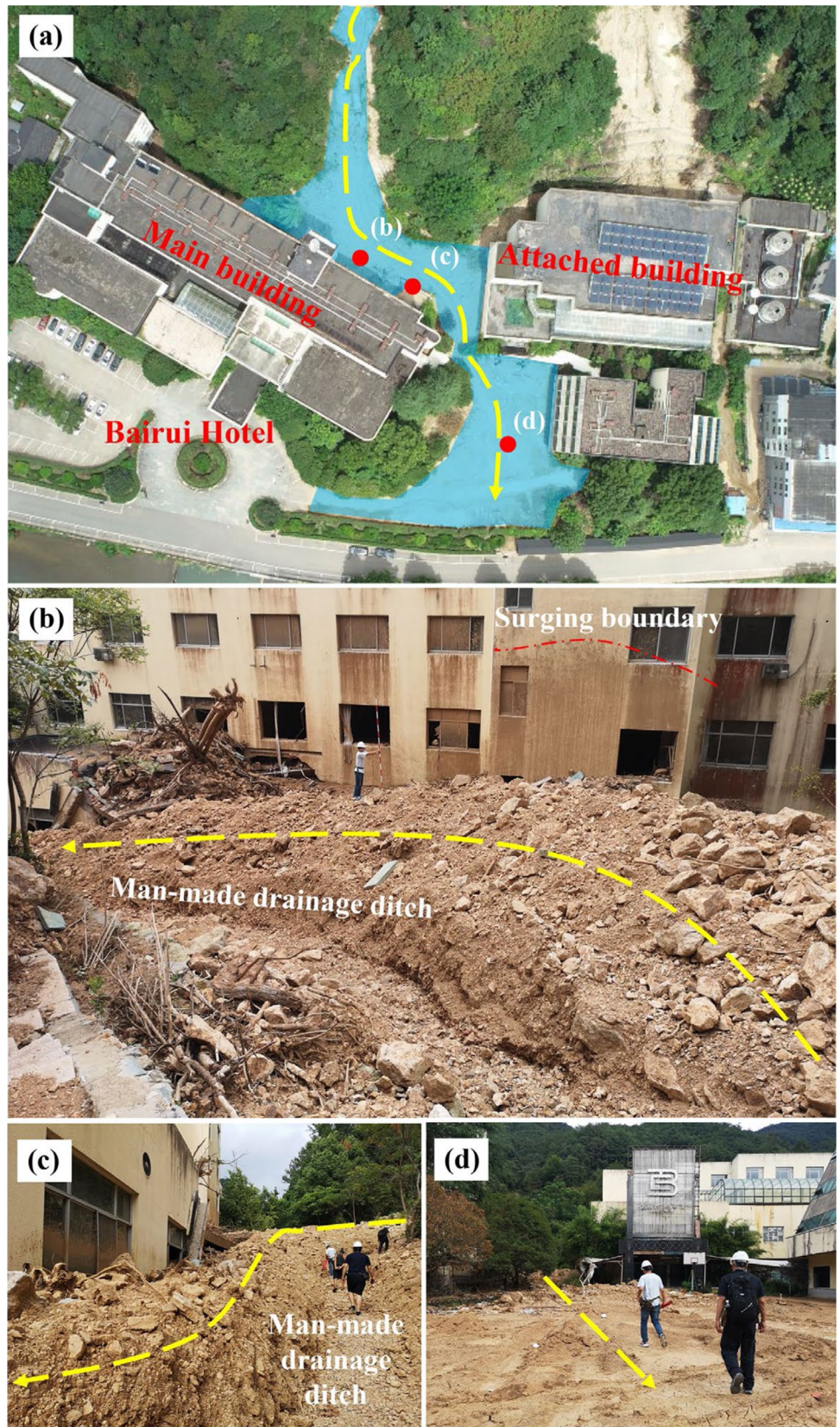
Primary tests of soil properties

To describe the initial properties of the eluvium in the source area, a sampling point was set in the DF3 source area (S2 in Fig. 9). First, several primary parameters, such as in situ density, water content and specific gravity, were tested using in situ and laboratory tests. The measured results are shown in Table 1. Their average values were 1143 kg/m³, 31.0% and 2.649, respectively. Furthermore, based on the above primary measured parameters, the void ratio and the degree of saturation of the sample were calculated as 1.319 and 63%, respectively. Therefore, it is indicated that the eluvium in the source area had a low dry density but a high water content in natural conditions.

Particle size distribution

The particle size distributions of the soil samples collected from DF1 (deposition front) and DF3 (source area) are illustrated by the gradation curves shown in Fig. 10. Grading characteristics of the soil samples, determined by the uniformity coefficient (C_u)/curvature coefficient (C_c), were 23.17/0.65 and 33.00/1.94, respectively. The grading property demonstrated that the eluvium in the rhyolitic area

Fig. 5 Deposition area and damages caused by DF2, including top view of deposition area (a) and detailed features of the damaged buildings (b–d)



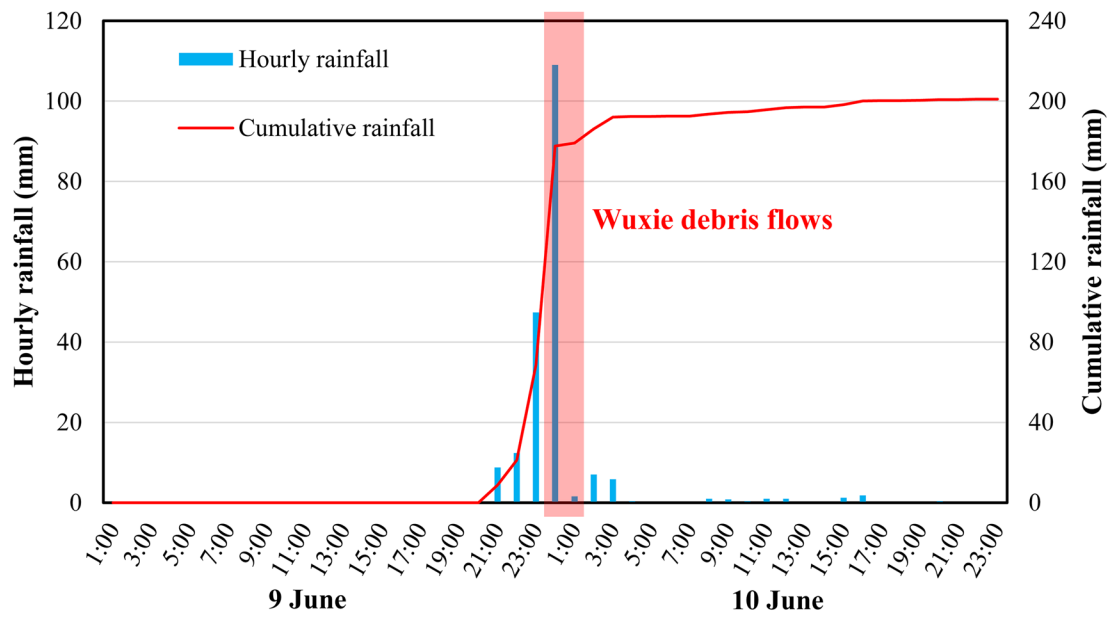


Fig. 6 Hourly rainfall and cumulative rainfall at the nearest meteorological station (WXSK)

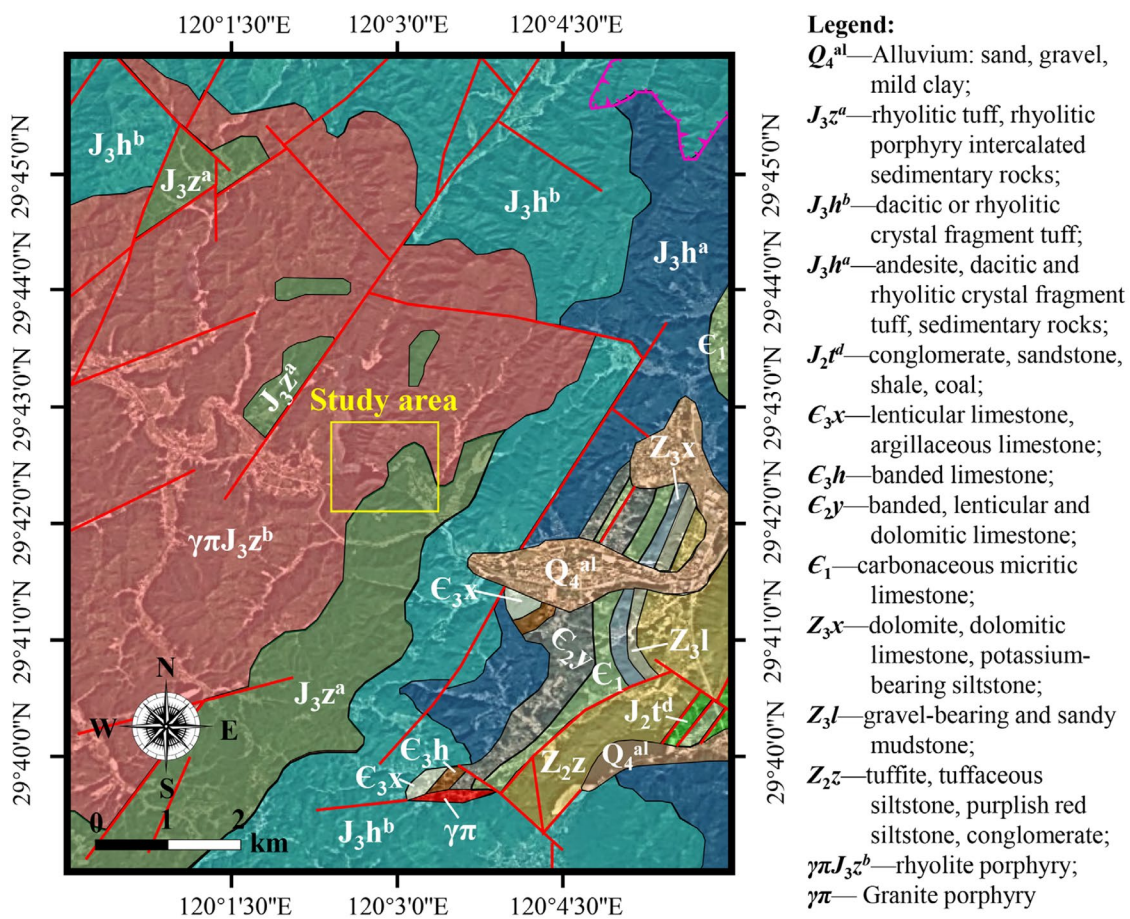


Fig. 7 Geological map (modified from Wu, 1979)

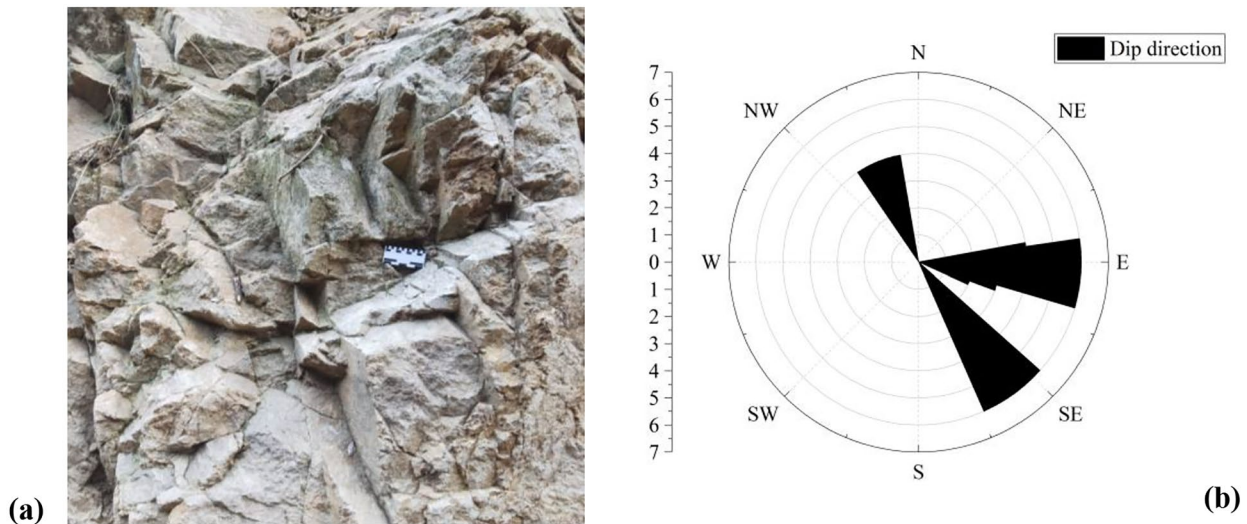


Fig. 8 Statistics of joints in the DF1 gully. **a** Statistic range (1.5 m × 1.5 m). **b** Rose diagram of dip direction

contained a larger proportion of coarse particles, as evidenced by the fact that d_{10} and d_{50} were 0.11 mm and 2.34 mm, respectively. The coarser eluvium had a higher permeability according to the relationship between soil permeability and grain size (Shepherd 1989). In addition, the two debris flows with similar gradation properties demonstrated that their difference in motion style was not determined by the grain size of the debris.

Hardness test of the soils

To measure the strength of the soils in the initial eluvium slope, a set of Yamanaka-style soil hardness tests were conducted in the DF3 resource area, as a representative example, and are shown in Fig. 11. The Yamanaka-style soil hardness test is a portable hardness test developed in Japan (Tanaka et al. 2004). There is a relationship between the unconfined compressive strength q_u and the contraction of spring x , modified from Tanaka et al. (2004), which can be written as Eq. (1).

$$q_u = \frac{100x}{0.815(40 - x)^2} \quad (1)$$

where x is the contraction of spring (mm) and q_u represents the unconfined compressive strength (kPa).

The test results for the soils taken from the DF3 source area are shown in Fig. 11b. It should be noted that the average unconfined compressive strength of the soil within a depth of 550 mm was about 250 kPa. There was an obvious fluctuation in the strength beneath the depth of 600 mm, reaching about 450 kPa, which might indicate that the source area of such debris flow was initiated by a shallow landslide with a thickness of about 600 mm.

Geomorphic characteristics of debris flows

Characteristics of DF1

DF1 had the longest movement distance from the main scarp to the toe of the deposition. Due to a high waterfall cliff in the middle of the gully (see Fig. 12), we could not access the source area. The UAV photographic technique was applied here to gain a fuller picture of the situation (Fig. 12), and hands-on inspections were conducted in the lower part of the debris flow (Fig. 14).

First, the DF1 gully, with a total dip length of 698 m and a dip direction of S38° E, was divided into six segments according to variations in dip directions. The movement path was mostly straight, except for a series of curves in the middle of the gully, from seg-b to seg-e. Within seg-a, the upper part of the gully, there was a source area and a large secondary shallow landslide that followed two parallel straight narrow gullies (see Fig. 12). DF1 was initiated by a small shallow slope failure. Its shape was an inverse trapezium with a top width of 21 m, bottom width of 17 m, dip length of 13 m and rake angle of 33°. Sliding out from the source area, the sliding mass was separated into two parts caught by two parallel gullies with a slope of 38° (Fig. 13) and a horizontal distance of about 100 m. One of the parallel debris flows (on the right side) triggered a large elliptic landslide (designated as the second landslide) at a steeper slope of 42° (Fig. 13). The elliptic exposed area had a major axis of 100 m and a minor axis of 28 m. After that, the slope of the gully was sharply reduced to 18° and extended to the end, with a small fluctuation in the range of 16–19°, except for the waterfall cliff (Fig. 13). In addition, a small side channel with a dip length of about 25 m and a width of 6 m merged into the main gully behind the waterfall cliff.

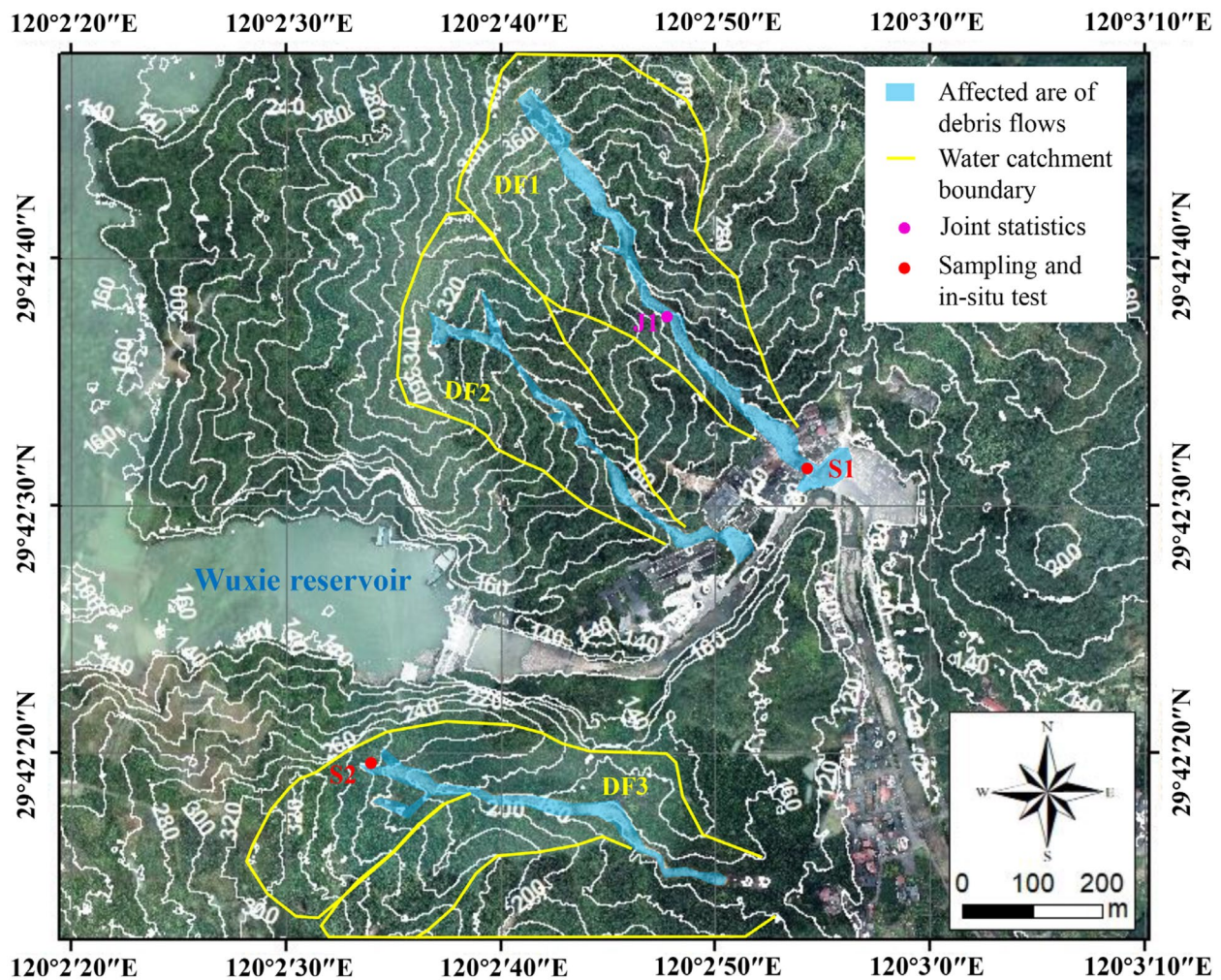


Fig. 9 Contour map of the study area (by SfM modelling)

From the waterfall cliff, the lower part of the DF1 gully is illustrated by the photographs shown in Fig. 14. The waterfall cliff (estimated height of 15 m) had clear scratches on the two sidewalls (Fig. 14a) and a little debris left at the bottom. This positioning indicates that the debris flow flew over the cliff at an extremely high velocity. Then, the high-impact energy of the debris flow eroded the gully bed covered by ancient diluvial depositions for about 2 m in depth, as shown in Fig. 14b. Next, the debris flow turned to the left bank (1.5 m-high lateral erosion) and excavated two buried

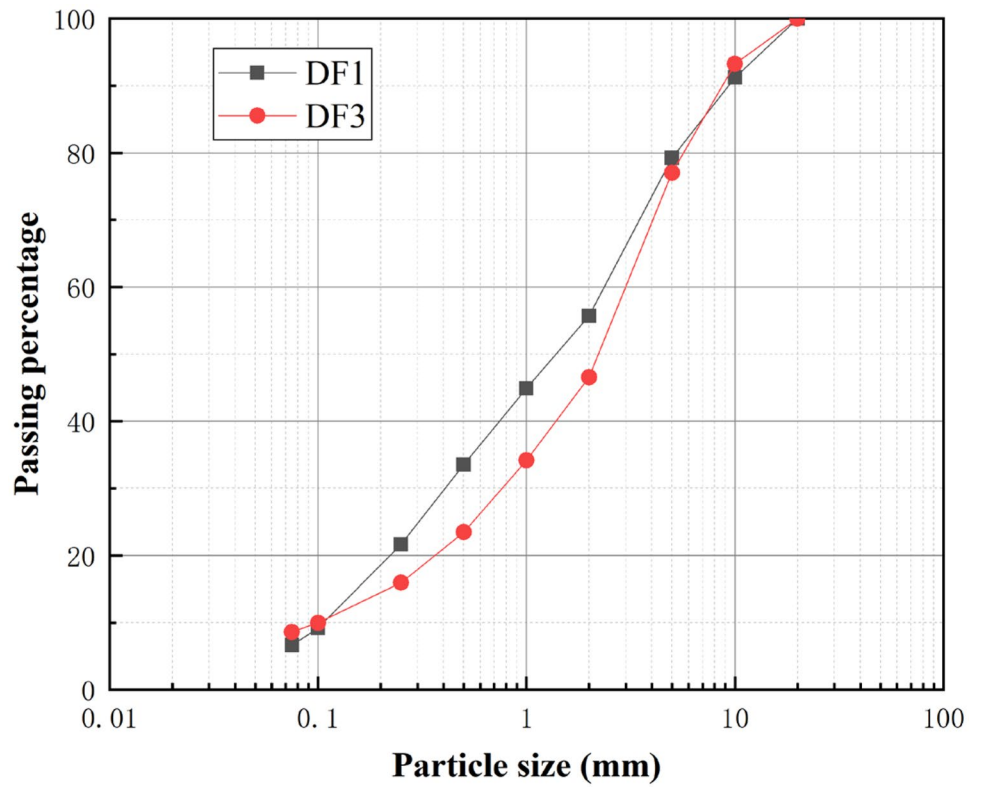
pipelines, as shown in Fig. 14c. Following the lateral erosion, a small cliff, about 2.5 m high, was created by the bed erosion caused by the debris flow at point (d) in Fig. 14i. From point (d) to point (f), there was an eroded curving channel with a depth of about 2 m. These segments were covered with abundant diluvium, which was partially eroded but not entirely removed by the impact of debris flow. However, from point (g) to the end of the gully (h), rare depositions were left and only boulders remained on the exposed rocky gully bed. The enlarged debris flow mostly removed the ancient diluvium in the lower part of the gully, which directly destroyed or severely damaged the downstream buildings.

Furthermore, there was a clear boundary between the transition zone and the deposition zone at the outlet of the gully, as indicated by a broken blue line in Fig. 14i. The size distributions of the material in the two zones were obviously different. This might have been caused by the width variation at the lower part of the gully. Abrupt increases in width would have reduced the velocity of the debris flow, which could have caused the separation of large boulders from the moving mass and kept them behind the finer debris. This phenomenon was also present in the second investigated gully (DF2), which is illustrated in Fig. 17n.

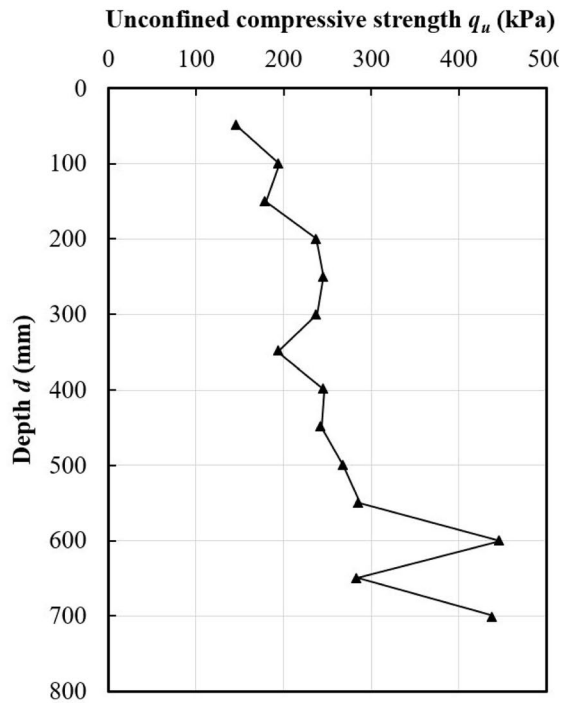
Table 1 Parameters of soil samples in the DF3 source area

Sample no	1	2	3	Average
Dry density, ρ_d (kg/m ³)	1245	1097	1088	1143
Water content, w (%)	26.7	30.3	36.7	31.0
Specific gravity, G_s	–	–	–	2.649
Void ratio, e	1.122	1.407	1.427	1.319
Degree of saturation, S_r (%)	63	57	68	63

Fig. 10 Particle size distribution of samples in DF1 and DF3



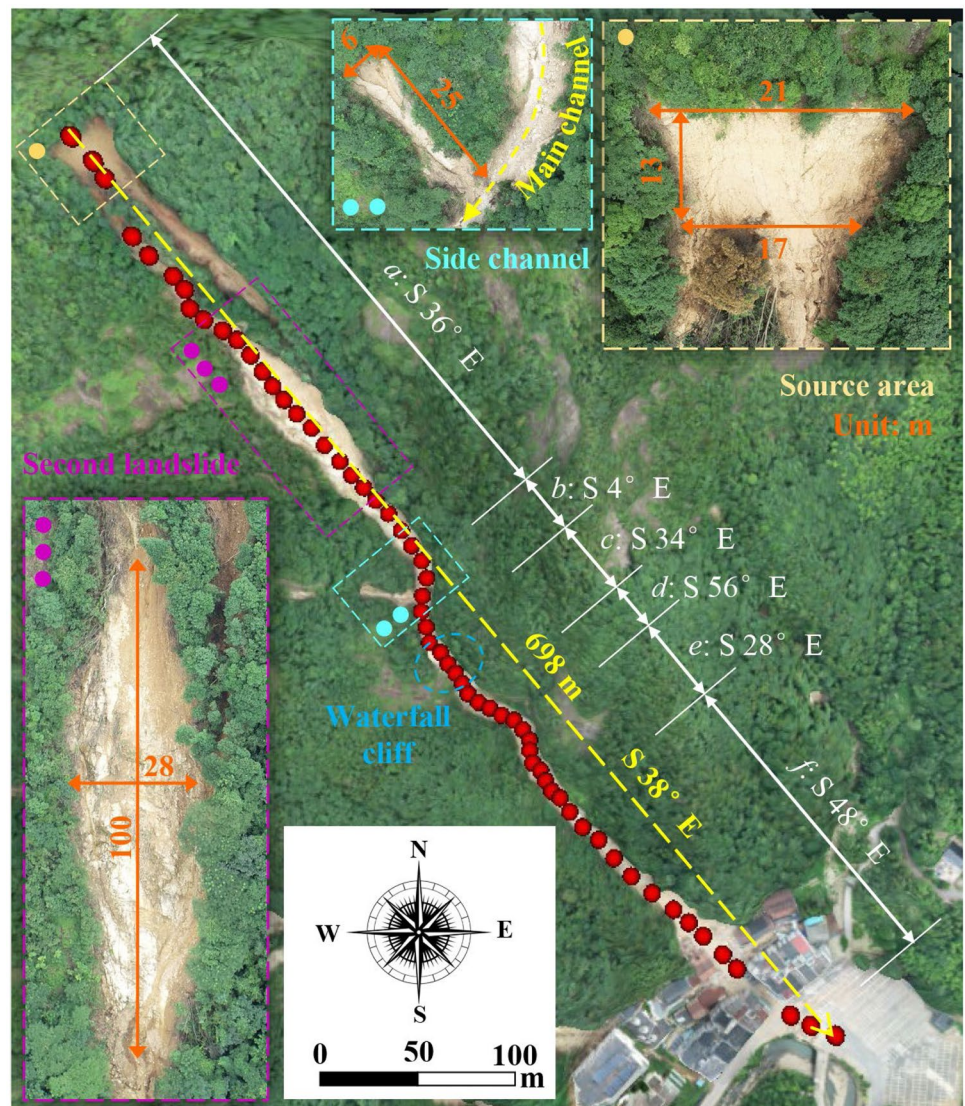
(a)



(b)

Fig. 11 Hardness test of the in situ soils at the DF3 source area: **a** testing ranges and **b** tested results of unconfined compressive strength along the depth

Fig. 12 Main geometric information of the DF1 gully: the overview image of the gully was acquired by SfM modelling, while three specified parts along the gully are illustrated using the UAV-captured photos and outlined in orange, light blue and purple dashes, respectively. This image splicing method is also used to describe the DF2 and DF3 gullies



Characteristics of DF2

DF2, the second investigated gully, had similar characteristics to DF1 overall but provided more specific details on the topographical variations of the debris flow gully. The gully was investigated thoroughly from the source area to the bottom along the red broken path shown in Fig. 15. The main geometrical features of DF2, including longitudinal and cross-sectional profiles, are illustrated in Fig. 16 as well as in the photographs in Fig. 17.

Overall, DF2 had a dip length of 535 m, a dip angle of $S52^\circ E$ and was divided into eight segments by the varied dip direction, except for the small deposition zone. There were two large source areas, three side landslides, six eroded cliffs and a variety of curving paths along the gully. The main source area consisted of three failed shallow landslides, as shown in Figs. 15 and 17b–d. The largest source area had a dip length (L) of 40 m, a width (W) of 15 m and a slope angle of 37° . The other two smaller source areas were estimated to be 20 m/15 m (L/W) and 10 m/10 m (L/W), respectively. They had a similar scarp height of 0.5–1.0 m to that of the largest source area. In terms of the parallel source area, a narrow straight gully towards $S18^\circ E$ had a

length of 70 m, an estimated width of 5 m and a slope angle of 33° . At the merging point of the two source areas (Fig. 17f), there was a small side landslide with a dip length of 22 m, an estimated width of 8 m and a slope angle of 34° . In addition to the above slope failures, two small shallow landslides occurred in the middle of the gully. These were approximately parallel to each other and had similar geometric parameters (see Fig. 15), with a large slope angle of over 40° in particular. Their failure should be attributed to slope cutting caused by the lateral erosion of the debris flow. The failed mass, in turn, blocked the gully and formed a natural dam. Finally, the collapse of the natural dam caused a large and deep area of erosion, as shown in Fig. 17l.

According to Fig. 16, the slope of the gully was initially 37° at the main source area and then reduced to 33° at the merging point. In this case, the slope of the main gully (33°) was the same as that of the parallel source gully (33°) and almost the same as that of the first-side landslides (34°) at the merging point. Then, the slope decreased to 27° involving two natural cliffs with an estimated height of 2–3 m. After that, the slope remained at 18° on average, with a slight fluctuation between 16 and 21° . Overall, DF2 was found to have a longitudinal profile similar to DF1.

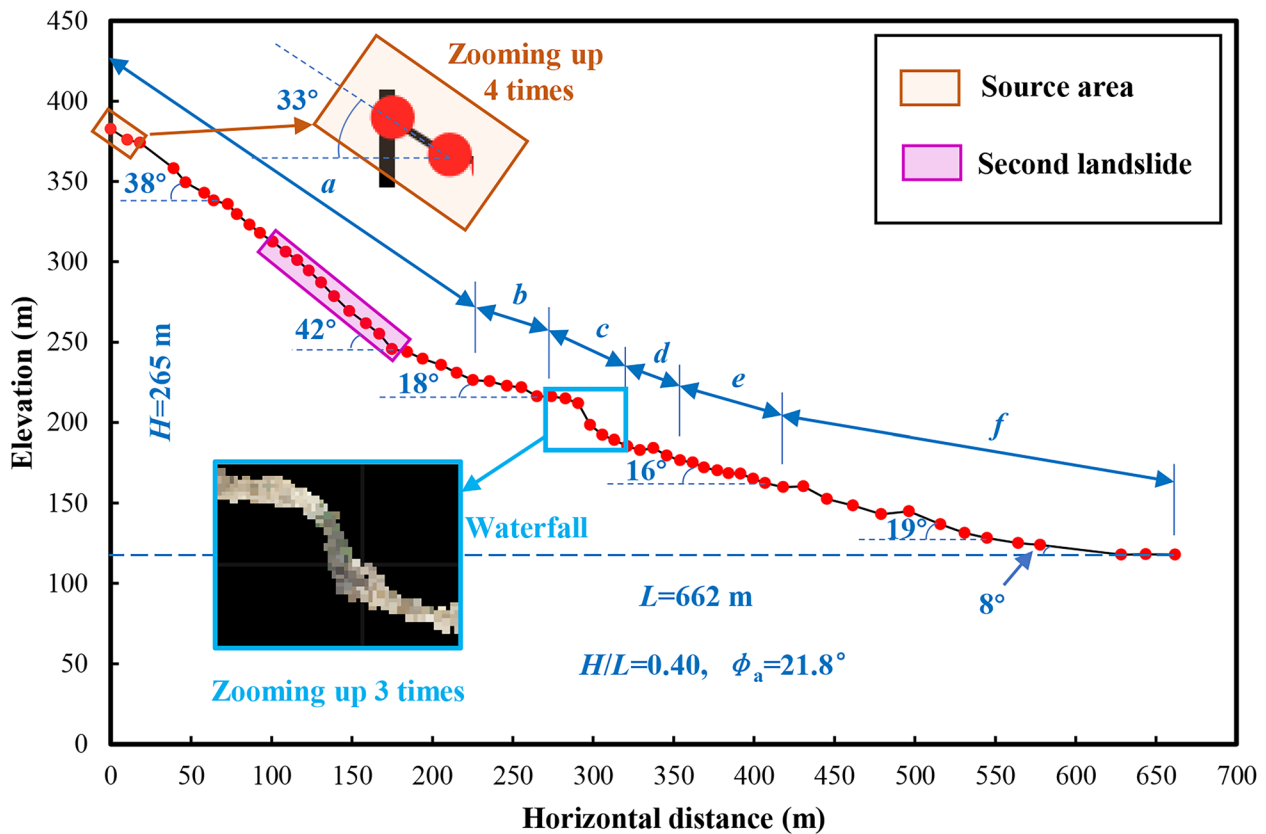


Fig. 13 Longitudinal profile of the DF1 gully

The DF2 gully had many more geometric variations, with three main features: the lateral curving path, the natural cliff and the cross-sectional shape. These are sketched in Figs. 16 and 17. Figure 16 shows two types of cross-sectional shapes: V-shape and U-shape. Most of the cross-sections of the gully were V-shaped and mainly located at curved segments, such as S-2, S-4, S-7 and S-9 (see Fig. 17g, j, m and p), in particular. In addition, S-5 and S-6, located at two large bed-eroded gullies (see Fig. 17k–l), were also determined to be V-shaped, although they each had a wide bottom. By contrast, the U-shapes, such as S-3, S-8 and S-10, are generally distributed along straight segments of the gully. In addition, there were six cliffs eroded by the debris flow and contributed significantly to the kinetic energy increase of the debris flow in turn. The mitigating countermeasures shown in Fig. 17o will be addressed in the ‘Discussion’ section.

The geometrical properties of the gullies had an obvious effect on the long-runout movement of the debris flows. According to the field investigation, the cliffs mostly followed curving segments with a V-shape. First, the curving path caused lateral erosion on the bank of the gully, which may have carved a V-shaped cross-section at the following segment. In a case like this, the velocity of the debris flow passing through the V-shaped cross increases, which can cause deep bed erosion, especially on the bed of an erodible diluvium. Meanwhile, bed erosion might, in turn, enlarge the eroded cliff. Finally, an increase in the moving mass from lateral erosion and bed erosion promotes the kinetic energy of the debris flow. Thus,

this process might serve as a reasonable explanation for the greater volumetric enlargement process of debris flow initiated by a small shallow landslide, especially in narrow gullies.

Characteristics of DF3

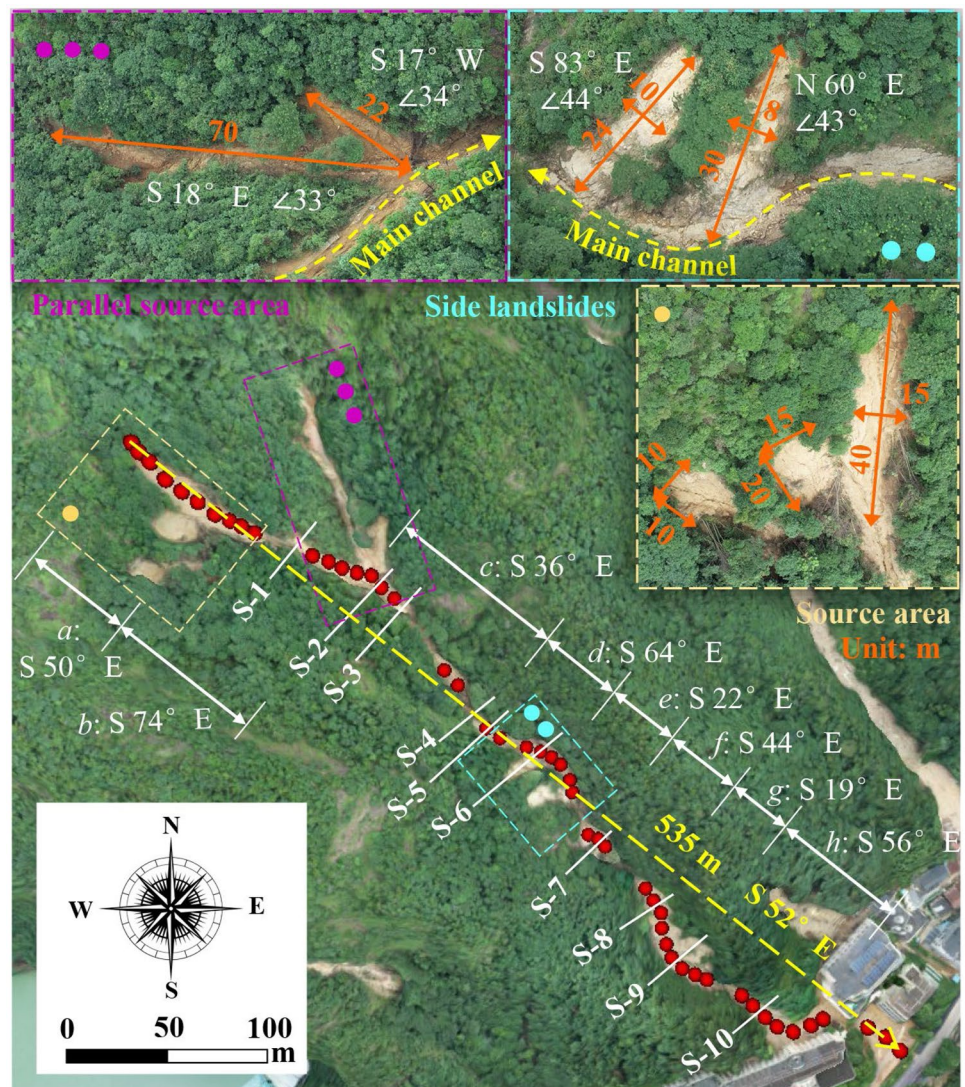
The third gully had different characteristics from the first two, as illustrated in Figs. 18, 19 and 20. The third gully had a dip length of 523 m and a dip direction of S72° E. It had a simple path that was only divided into three segments. Seg-a included the main source area, transition zone and part of the deposition zone, while seg-b and seg-c were fully located in the deposition zone. Two landslides of different sizes occurred in the source area. The larger landslide in the main source area consisted of two segments, with an average dip length of about 60 m. The upper part in the initially failed zone had an estimated width of 10 m and a slope angle of 32° (see Fig. 19), while the lower part had a larger width of 16 m but a gentler slope angle of 25°. The smaller landslide in the parallel source area had a dip length of 70 m and a width of 20 m, according to the SfM modelling. Sliding out from the steeper source area, the debris flow entered a gentle transition zone with a slope that ranged from only 13 to 9°. In the deposition zone, the slope of the gully gradually decreased from 6 to 4° at the end (see Fig. 19).

DF3 had a larger water catchment area (Fig. 9) than DF1 and DF2. According to Fig. 18, two slightly failed gullies merged into the upper part of the transition zone. Although they did not import as



Fig. 14 Photographs describing the DF1 gully from the waterfall cliff to the gully outlet. These detailed features are illustrated by photos (a–h) taken along the investigation path shown in photo (i)

Fig. 15 Topographic characteristics of the DF2 gully



much debris into the mainstream, these gullies may have contributed a great amount of water to the main gully. If this were the case, the large water catchment would have provided abundant water in the transition and deposition zones, which shifted the diluvium into a fully saturated state. Once a failed debris mass has slid across or flowed over the saturated soils, the shear strength of the soil may be reduced sharply because of shear liquefaction, an idea proposed by Sassa et al. (1996). This liquefaction might explain why the debris flow had a long-runout distance, even in the presence of smaller elevation differences.

A detailed field investigation from the source area to the deposition front was also undertaken (see Fig. 20). First, in addition to a shallow landslide (Fig. 20b) occurring at the source area, there was a small slope failure on its left side (Fig. 20d) and a small crack between them (Fig. 20c). Figure 20e shows that there was an outcropped rock bed on the right side of the gully. After sliding out of the main source area, the debris mass merged with another mass from the parallel source area at confluence, as depicted in Fig. 20f. Due to a small curve at confluence, the rapidly moving mass heavily

eroded the right bank of the gully (Fig. 20g) and the downstream diluvial depositions (Fig. 20h). At the end of the transition zone, the kinetic energy may have been sharply reduced before deposition, as evidenced by the fact that the reeds were inclined but not removed (Fig. 20i). Meanwhile, the inclined but unfractured reeds suggest that the debris flow had high fluidity and low frictional resistance when sliding over the grass surface, according to the observations made by Wang et al. (2002). Additionally, the left reeds demonstrated that the diluvium of the gully had a high water content and may even have been fully saturated, which might have been the key factor contributing to the long-runout distance of the debris flow. Furthermore, as the debris flow entered the deposition zone, the woods and coarse sands were gradually separated from the debris mass (Fig. 20j–m). The curved gully separated the wood from the moving debris (Fig. 20j–k). Finally, the debris flow, a mixture of wood, fine gravels and soils, halted in the middle of an artificial dammed lake and formed a flat deposition ground, as shown in Fig. 20l. In sum, DF3 was vastly different from DF1 and DF2 due to its high fluidity, long-runout distance and particularly its wide and smooth gully.

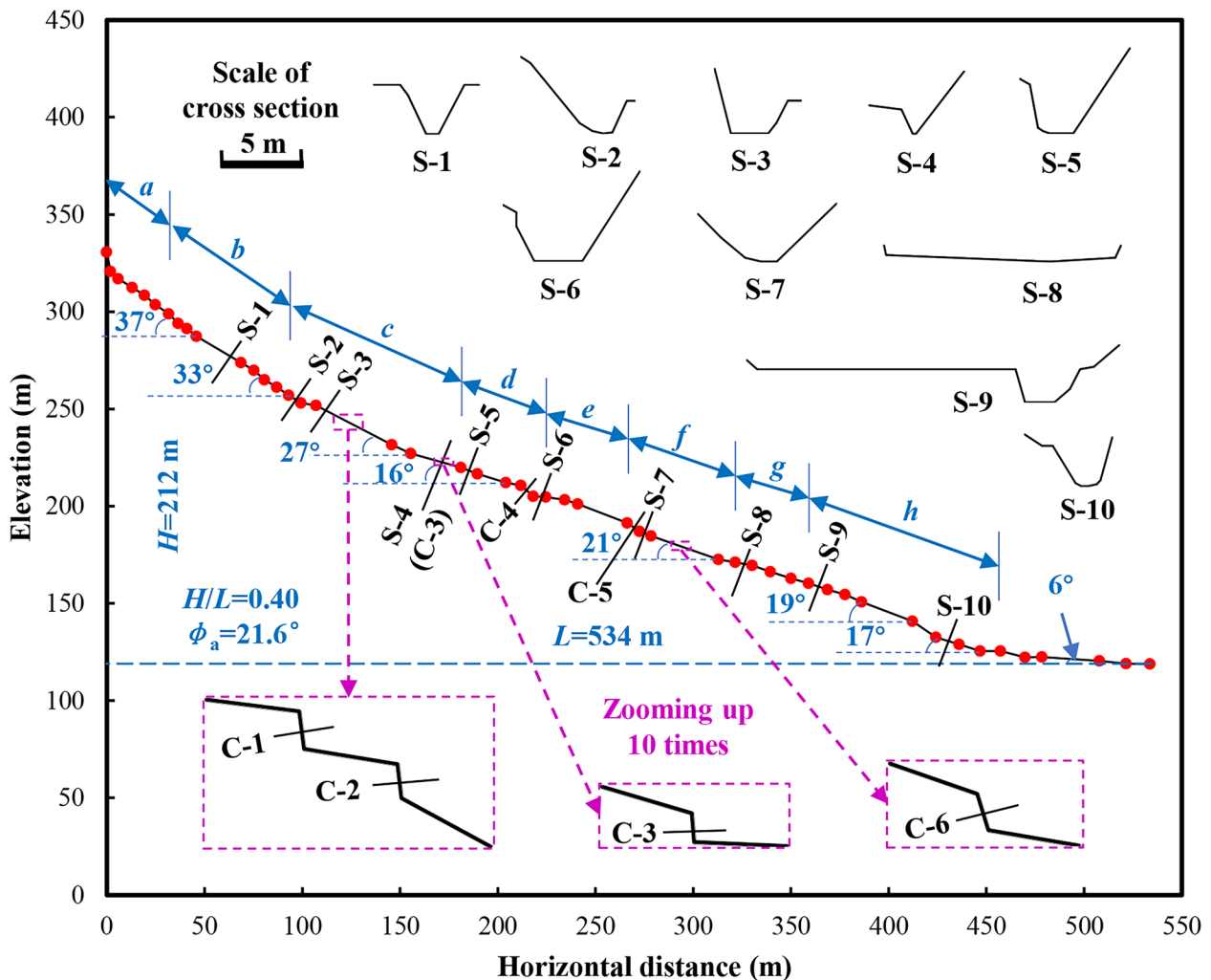


Fig. 16 Longitudinal section and cross-section of DF2. 'S-' and 'C-' represent cross-sections of 'slope' and 'cliff' positions, respectively

Discussion

Potential failure mechanism of the source area

Overall, the rhyolitic mountainous area generally has steep slopes and shallow eluvium, especially in the upper part of the mountains. This is due to the strong anti-weathering capabilities of rhyolite. A steep slope is a primary geomorphic condition for the occurrence of initial landslides. According to the field investigations, all three investigated gullies initially failed at slopes over 32°. Meanwhile, the initial eluvial soils in the source areas had rich coarse grains, which indicated that the eluvium had high permeability, according to Shepherd (1989). In fact, the higher permeability of soil, which suggests that the water inside the soil could be drained more quickly, was found to have more active effect on the stability of a slope in ordinary precipitation conditions. In this case, a slope covered by eluvium with high permeability might not easily fail in low-intensity rainfall, despite its long duration. However, once the infiltration rate of rainfall is larger than the drainage rate of the eluvial soil, the soil gradually becomes saturated, resulting in an

increase in pore water pressure. Thus, the effective stress of the soil will be reduced, which is the major contributing factor to the loss of the shear strength of the soil. Therefore, in this rhyolitic eluvium with a tiny proportion of fine grains, the initial shallow landslides in those steep slopes were triggered by extremely heavy precipitation, which caused the infiltration rate to exceed the drainage rate of the soil. The failed debris mass rushed down along the gullies with high kinetic energy and gradually became large debris flows.

Significance of vegetation on soil stabilisation in the source area

The contribution of plants to the stabilisation of slope has been introduced in various studies, as well as in practical projects (Vergani et al. 2017; Löbmann et al. 2020). The field investigation of DF3 found a great number of roots embedded into the eluvial soils, as shown in Fig. 21, which enforced the shear strength of the eluvium. In this case, the anti-erosion capability of the soils was strengthened as expected, which prevented bed erosion and lateral erosion of the debris flows to some extent. The significance of plants with



Fig. 17 Photographs describing the DF2 gully from the main source area to the toe. The spliced image (a) illustrates the investigated positions of the detailed features from (b) to (p) along the gully

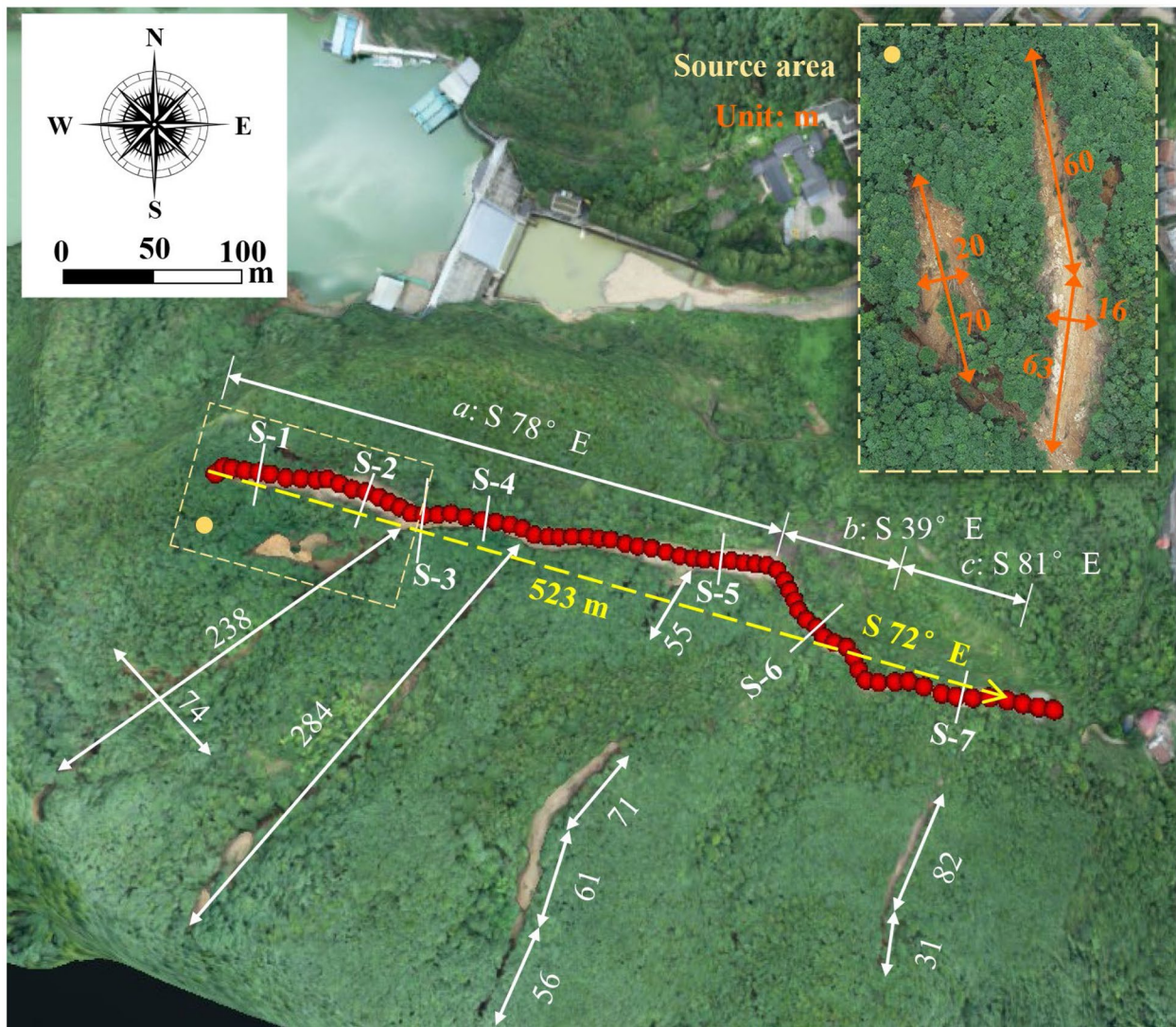


Fig. 18 Topographic properties of DF3 (SfM modelling)

well-developed roots on the reduction of debris flows should be studied further, especially in areas prone to shallow slope failures.

Countermeasures for mitigating debris flows

Reasonable and effective countermeasures, based on movement characteristics of the debris flows, are of great importance for the mitigation of geo-disasters. During the field investigations, two preventative structures were found in DF2 and DF3, as illustrated in Figs. 22 and 23, respectively. The first was a composite structure consisting of three barrier walls and two side walls. The walls were made of debris stones without any concrete or rebars. Although this area was damaged in this disastrous event, a large amount of debris mass, especially for the coarser boulders, was

halted here. The multiple walls formed an artificial terrace with a wide, flat platform on top. In this case, the sudden widening of the gully at the flat platform may have sharply reduced the kinetic energy of the debris flow and quickly drained water from the debris mass, causing the debris flow to mostly stop here. In the same way, the second structure, a single earth dam with a drainage channel, also reduced the gradient of the gully at the end of DF3 and effectively prevented debris flow. The long and gentle segment behind the dams provided enough space for the deceleration of the rapid mass movement, which protected the downstream buildings and the lives of the people within them. Effective countermeasures such as these are necessary to mitigate future geo-disasters. Additionally, extreme weather conditions should be taken into account when designing structures for disaster mitigation in the future.

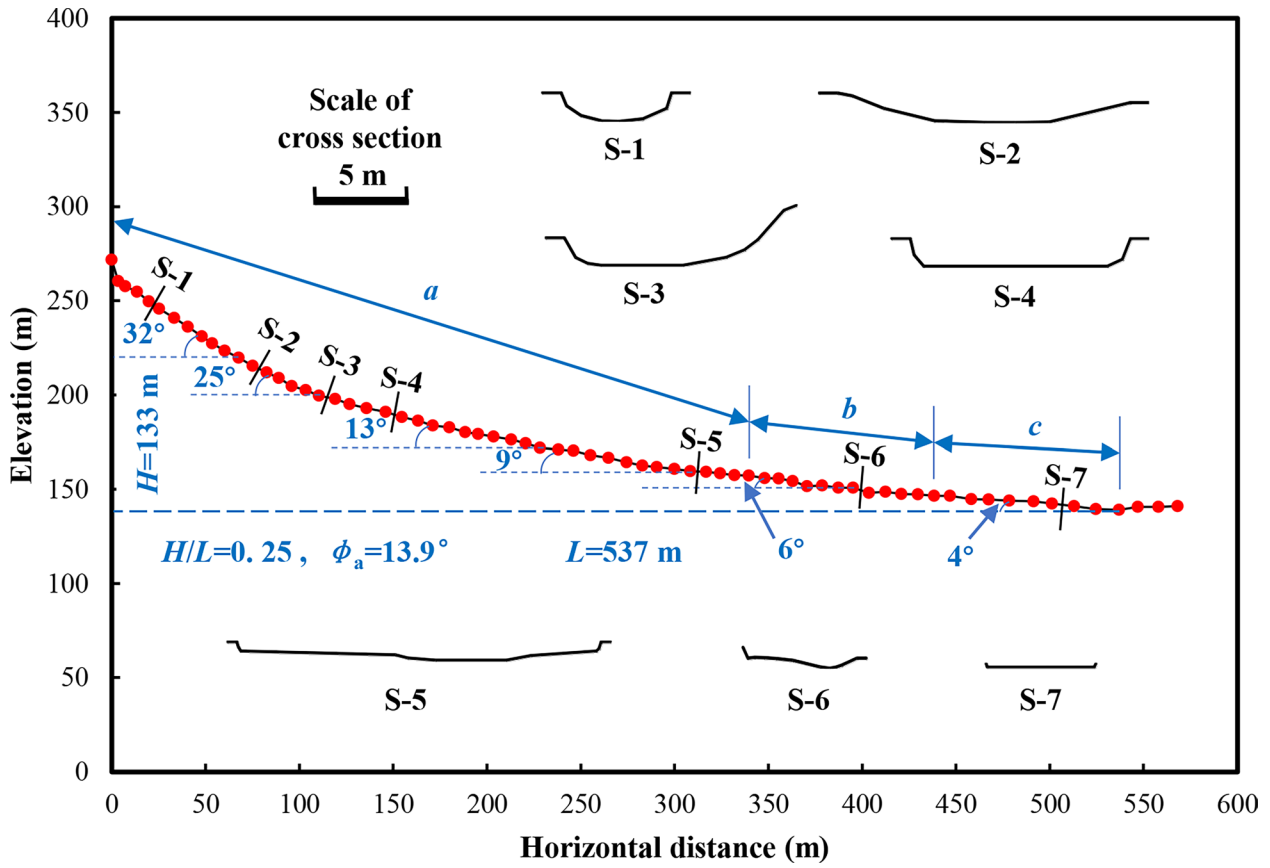


Fig. 19 Longitudinal and cross-sectional profiles of DF3

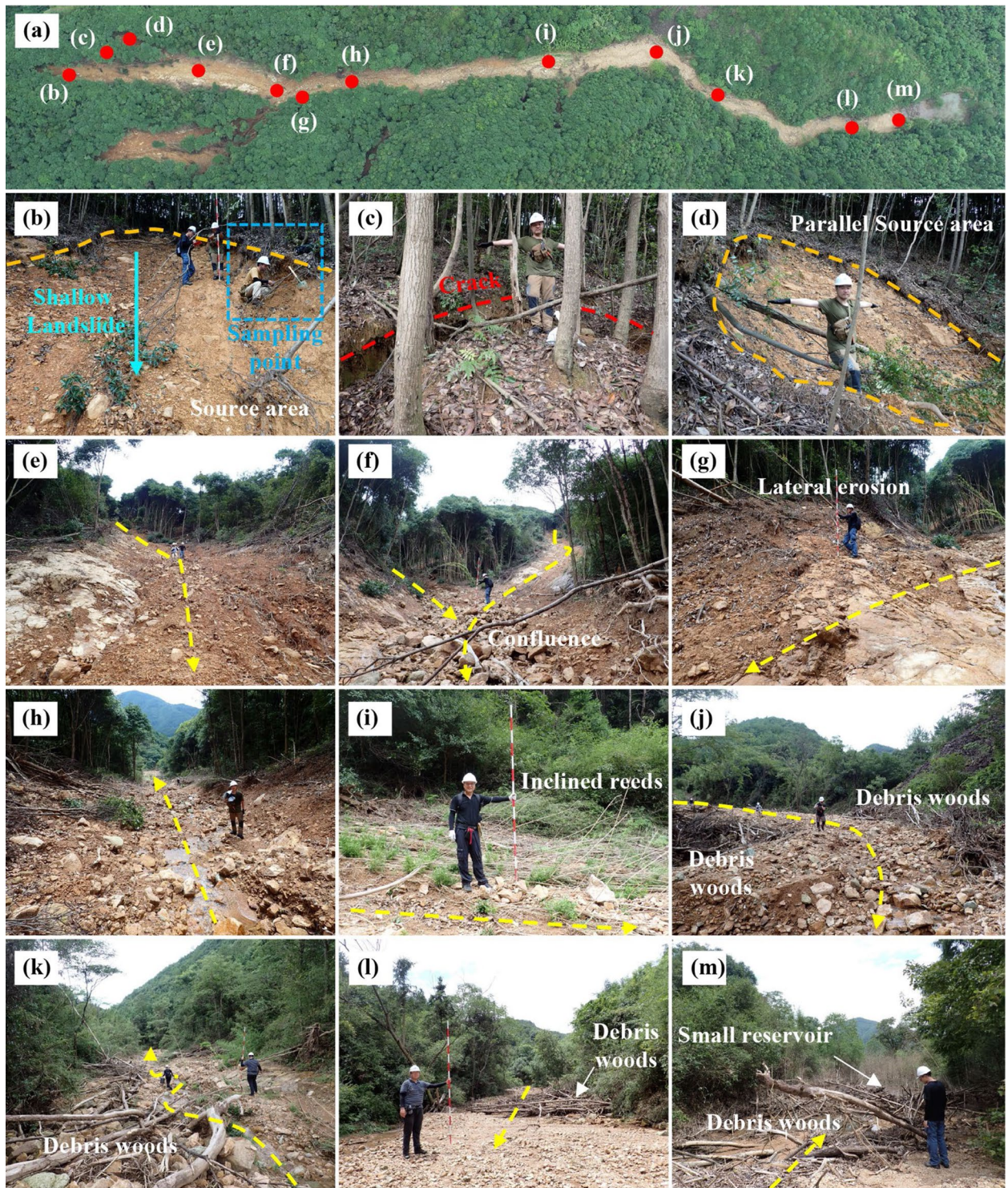


Fig. 20 Photographs describing the geological features of the DF3 gully from top to bottom. The UAV-captured image (a) illustrates the positions of the investigated features shown in (b–m)

Fig. 21 Root of the plants left in the eluvium of the upper DF3 gully. **a** A single broken root embedded into the gully bed; **b** exposed roots stayed in the table eluvium

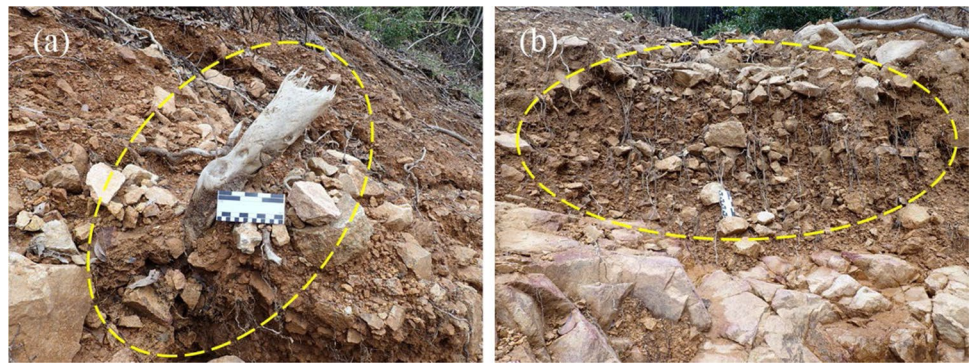


Fig. 22 Debris stone barrier walls behind the hotel



Fig. 23 Constructed earth dam behind the local village

Conclusion

Based on detailed field investigations, the key aspects of the Wuxie debris flows are summarised as follows:

- (1) In a rhyolitic eluvium with a large proportion of coarse grains, steep slopes played a significant role in the initiation of debris flows. Also significant was the extreme precipitation, which had an infiltration rate exceeding the drainage rate of the soil.
- (2) The varied topographic features, such as the curving path, naturally eroded cliffs and cross-sectional shape, as well as the abundant water supplements in transition zones, contributed greatly to the long-runout movement of debris flows. In addition, massive, dominant diluvial depositions in the gully were also significant factors because they increased the kinetic energy of the debris flows, contributing to their mass enlargements.
- (3) Reasonable countermeasures and land use would have worked effectively to reduce and prevent these fluidised geo-disasters. Furthermore, extreme weather conditions that occur with increasing frequency due to global climate variation should be considered to implement mitigating countermeasures in the future.

Acknowledgements

The Hydrological Centre of Zhuji Water Resource Bureau provided the meteorological data. Mr. Ye Chen of Tongji University participated in the field investigations.

Funding

This study was supported by the National Natural Science Foundation of China (Grant No. 42107170), the China Postdoctoral Science Foundation (Grant No. BX2021214 and 2021M702493), the Shanghai Post-doctoral Excellence Program (Grant No. 2020423) and the Fundamental Research Funds of China for the Central Universities.

Declarations

Conflict of interest The authors declare no competing interests.

References

- Achu AL, Joseph S, Aju C, Mathai J (2021) Preliminary analysis of a catastrophic landslide event on 6 August 2020 at Pettimudi, Kerala State, India. *Landslides* 18:1459–1463. <https://doi.org/10.1007/s10346-020-01598-x>
- Chang M, Liu Y, Zhou C, Che H (2020) Hazard assessment of a catastrophic mine waste debris flow of Hou Gully, Shimian. *China Engineering Geology* 275:105733. <https://doi.org/10.1016/j.enggeo.2020.105733>
- Cuomo S (2020) Modelling of flowslides and debris avalanches in natural and engineered slopes: a review. *Geoenvironmental Disasters* 7:1. <https://doi.org/10.1186/s40677-019-0133-9>
- Dogliani A, Casaglini N, Nocentini M, Sdao F, Simeone V (2020) The landslide of Pomarico, south Italy, occurred on January 29th, 2019. *Landslides* 17:2137–2143. <https://doi.org/10.1007/s10346-020-01455-x>
- Guo J, Yi S, Yin Y, Cui Y, Qin M, Li T, Wang C (2020) The effect of topography on landslide kinematics: a case study of the Jichang town

- landslide in Guizhou, China. *Landslides* 17:959–973. <https://doi.org/10.1007/s10346-019-01339-9>
- Hotta N, Iwata T, Suzuki T, Sakai Y (2021) The effects of particle segregation on debris flow fluidity over a rigid bed. *Environ Eng Geosci* 27(1):139–149. <https://doi.org/10.2113/EEG-D-20-00106>
- Igwe O, Sassa K, Wang F (2006) The influence of grading on the shear strength of loose sands in stress-controlled ring shear tests. *Landslides* 4:43–51. <https://doi.org/10.1007/s10346-006-0051-2>
- Jeong S, Kim Y, Lee J, Kim J (2015) The 27 July 2011 debris flows at Umyeonsan, Seoul, Korea. *Landslides* 12:799–813. <https://doi.org/10.1007/s10346-015-0595-0>
- Löbmann MT, Geitner C, Wellstein C, Zerbe S (2020) The influence of herbaceous vegetation on slope stability—a review. *Earth Sci Rev* 209:103328. <https://doi.org/10.1016/j.earscirev.2020.103328>
- McFall B, Mohammed F, Fritz H, Liu Y (2018) Laboratory experiments on three-dimensional deformable granular landslides on planar and conical slopes. *Landslides* 15:1713–1730. <https://doi.org/10.1007/s10346-018-0984-2>
- Peng J, Fan Z, Wu D, Zhuang J, Dai F, Chen W, Zhao C (2015) Heavy rainfall triggered loess–mudstone landslide and subsequent debris flow in Tianshui, China. *Eng Geol* 186:79–90. <https://doi.org/10.1016/j.enggeo.2014.08.015>
- Plummer C, Carlson D, Hammersley L (2015) *Physical geology* (fifteenth edition). McGraw-Hill Education, United States
- Samodra G, Hadmoko DS, Wicaksono GN, Adi IP, Yudinugroho M, Wibowo SB, Suryatmojo H, Purwanto TH, Widartono BS, Lavigne F (2018) The March 25 and 29, 2016 landslide-induced debris flow at Clapar, Banjarnegara, Central Java. *Landslides* 15:985–993. <https://doi.org/10.1007/s10346-018-0958-4>
- Sassa K, Fukuoka H, Scarascia-Mugnozza G, Evans S (1996) Earthquake-induced-landslides: distribution, motion and mechanisms. *Soils Found* 36:53–64. https://doi.org/10.3208/sandf.36.Special_53
- Setiawan H, Wilopo W, Wiyoso T, Fathani TF, Karnawati D (2019) Investigation and numerical simulation of the 22 February 2018 landslide-triggered long-traveling debris flow at Pasir Panjang Village, Brebes Regency of Central Java, Indonesia. *Landslides* 16:2219–2232. <https://doi.org/10.1007/s10346-019-01245-0>
- Shepherd RG (1989) Correlations of permeability and grain size. *Groundwater* 27:633–638. <https://doi.org/10.1111/j.1745-6584.1989.tb00476.x>
- Tanaka Y, Wang F, Nakamura K, Matsumoto T (2004) Sliding mechanism of the Yamashina flowslide triggered by continual rainfall in Kanazawa City, Japan. *Proc. 15th South-East Asian Geotechnical Conference—Development in Geot. Engineering for Practice, Bangkok* 1:331–336
- Vergani C, Giadrossich F, Buckley P, Conedera M, Pividori M, Salbitano F, Rauch HS, Lovreglio R, Schwarz M (2017) Root reinforcement dynamics of European coppice woodlands and their effect on shallow landslides: a review. *Earth Sci Rev* 167:88–102. <https://doi.org/10.1016/j.earscirev.2017.02.002>
- Wang F, Sassa K, Wang G (2002) Mechanism of a long-runout landslide triggered by the August 1998 heavy rainfall in Fukushima Prefecture, Japan. *Eng Geol* 63:169–185. [https://doi.org/10.1016/s0013-7952\(01\)00080-1](https://doi.org/10.1016/s0013-7952(01)00080-1)
- Wang F, Wu Y, Yang H, Tanida Y, Kamei A (2015) Preliminary investigation of the 20 August 2014 debris flows triggered by a severe rainstorm in Hiroshima City. *Japan Geoenvironmental Disasters* 2:17. <https://doi.org/10.1186/s40677-015-0025-6>
- Wang G, Sassa K, Fukuoka H (2003) Downslope volume enlargement of a debris slide–debris flow in the 1999 Hiroshima, Japan, rainstorm. *Eng Geol* 69:309–330. [https://doi.org/10.1016/s0013-7952\(02\)00289-2](https://doi.org/10.1016/s0013-7952(02)00289-2)
- Wu M (1979) Regional hydrogeological survey report of Zhuji H-51-19 1/200,000. China National Geological Reference Library. [https://doi.org/10.35080/n01.c.61690\(inChinese\)](https://doi.org/10.35080/n01.c.61690(inChinese))
- Yang H, Wang F, Miyajima M (2015a) Investigation of shallow landslides triggered by heavy rainfall during typhoon Wipha (2013), Izu oshima Island. *Japan Geoenvironmental Disasters* 2:15. <https://doi.org/10.1186/s40677-015-0023-8>
- Yang H, Wang F, Villimek V, Araiba K, Asano S (2015b) Investigation of rainfall-induced shallow landslides on the northeastern rim of Aso caldera, Japan, in July 2012. *Geoenvironmental Disasters* 2:20. <https://doi.org/10.1186/s40677-015-0028-3>

- Zhao B, Zhang H, Liao H, Li W, Su L, He W, Zeng L, Qin H, Dhital MR (2021) Emergency response to the reactivated Aniangzhai landslide resulting from a rainstorm-triggered debris flow, Sichuan Province, China. *Landslides* 18:1115–1130. <https://doi.org/10.1007/s10346-020-01612-2>
- Zheng R, Zheng Y, Cong L, Choi J, Jung H (2020) Climate adaptive design improvement strategies of traditional dwellings in southern Zhejiang for the plum rain season considering comfort conditions. *Energies* 13(6):1428. <https://doi.org/10.3390/en13061428>
- Zhou G, Cui P, Tang J, Chen H, Zou Q, Sun Q (2015) Experimental study on the triggering mechanisms and kinematic properties of large debris flows in Wenjia gully. *Eng Geol* 194:52–61. <https://doi.org/10.1016/j.enggeo.2014.10.021>

Fawu Wang · Kongming Yan (✉) · **Kounghoon Nam · Guolong Zhu · Xingliang Peng · Zixin Zhao**

College of Civil Engineering, Tongji University, Shanghai 200092, China

Email: kmyan@tongji.edu.cn

Fawu Wang

Key Laboratory of Geotechnical and Underground Engineering, Ministry of Education, Tongji University, Shanghai 200092, China